Macromolecules

Article

pubs.acs.org/Macromolecules

Study of the Mechanisms of Filler Reinforcement in Elastomer Nanocomposites

Alexey A. Gavrilov,*[,†,‡] Alexander V. Chertovich,[†] Pavel G. Khalatur,[‡] and Alexei R. Khokhlov[†,‡]

[†]Physics Department, Lomonosov Moscow State University, 1-2 Leninskiye Gory, Moscow 119991, Russia

[‡]Institute for Advanced Energy Related Nanomaterials, University of Ulm, Albert-Einstein-Allee 47, Ulm D-89069, Germany

ABSTRACT: We performed a large-scale dissipative dynamics simulation to study the structural changes in unfilled and filled elastomers during uniaxial deformation, which helped to shed some light on the underlying reasons of filler reinforcement in rubber nanocomposites. Equilibrium stress−stain curves for different cross-linker concentrations and filler content were obtained, and their features were compared to the experimental data. Dependences of segmental orientation on deformation and true stress were studied; these dependences are discussed in the light of theoretical predictions and available experimental data. The structural changes in the deformed state were studied as well, namely, the dependences of mean end-to-end distance on the subchain length. For the filled elastomers it was found that in the matrix there are several sets of subchains with distinct properties. Part of the subchains which are not connected to the filler particles are deformed slightly more than in the unfilled matrix; the subchains connected to the filler particles are deformed significantly more. This "separation" is the main reason for reinforcement; its influence on the properties of the filled systems is discussed. In addition, the effect of the network topology (randomly cross-linked, end-linked, ideal diamond-like) on the mechanical properties of unfilled elastomers was studied.

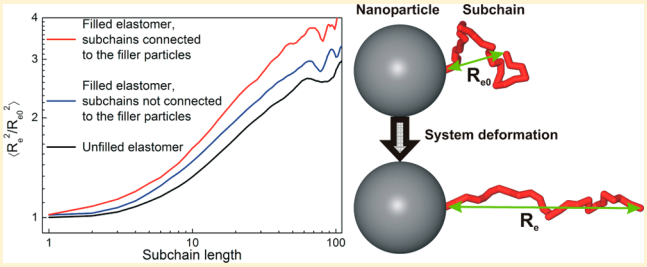

1. INTRODUCTION

Polymer networks are composed of polymer chains that are cross-linked to each other, thereby forming a giant three-dimensional macromolecule. Weakly cross-linked polymer networks (i.e., those in which the distance between cross-links along the polymer chains is much more than one statistical segment), which are usually called elastomers, have a property of rubber elasticity, i.e., the ability to undergo large reversible deformations under the action of a relatively small external force. The main feature of this type of elasticity is that it has an entropic nature; thus, unlike other solids (for example, metals), where the main mechanism of elasticity is energetic, rubber matrixes become stiffer upon heating.

A detailed understanding of the mechanisms of rubber elasticity of real polymer networks remains one of the most interesting problems in polymer physics. Over the past years, numerous attempts to develop a good analytical model have been made,[1−4] but they have had only partial success. There are many models of rubber elasticity, but they often conflict with one another and most of them are phenomenological in character and do not explicitly take into account the network structure. Modern experimental techniques, for example NMR and X-ray scattering, can be a powerful tool to study the properties of elastomers in more details (for example, segmental orientation);[5] however, the detailed molecular-level structure and its influence on the properties are beyond their reach. On the other hand, computer simulation allows one to study the structure of a network explicitly. Because of rather slow relaxation processes and big system volumes required to have good statistics, the most suitable way is to utilize coarse-grained (CG) models. After the pioneer works of Kremer and Grest,[6,7] in which the statistical properties (block-length distribution, etc.) and critical properties (percolation thresholds) were studied, there have been a number of studies dedicated to CG simulations of rubber-like materials. Using the model developed by Kremer and Grest, Everaers and Kremer[8] calculated the stress−strain curves for interpenetrating diamond-like networks and for the first time showed that entanglements have significant influence on the mechanical properties. Svaneborg et al.[9,10] showed that the double-tube model[2] can be successfully utilized to describe the microscopic behavior and stress−strain response of both end-linked and random-linked networks; in the subsequent work[11] it was shown that the contributions of cross-links and entanglements to the elasticity can be described in terms of the simple elasticity theory and the slip-tube model,[1] respectively.

Inclusion of solid particles into elastomer matrixes can tune many properties, but the most common is the mechanical behavior; such systems are called composites (or nanocomposites, if the filler particles have nanoscale size). Nowadays, carbon nanotubes[12] and spherical particles (for example, synthetic silica nanoparticles)[13] attract main attention

Received: May 8, 2014
Revised: June 19, 2014
Published: July 14, 2014

   dx.doi.org/10.1021/ma500947g | *Macromolecules* 2014, 47, 5400−5408

as fillers. Such elastomer composite materials, in which inorganic particles are dispersed in cross-linked polymer matrixes, have been the subject of extensive research during several past decades; however, despite the experimental and theoretical efforts the complete picture of reinforcement remains unclear. There are several mechanisms which have been proposed to explain reinforcement. One of the mechanisms assumes that changes in the matrix properties close to the filler surfaces (namely, an increased density of trapped entanglements) play the main role in the reinforcement.[14] However, there is no direct observation of the increase in the density of entanglements; moreover, some molecular dynamics studies[15] show that while spherical nanoparticles act as attractors for entanglements, the density of chain entanglements in the vicinity of the particles is reduced. Another possible mechanism of reinforcement is formation of filler network, which results in transmission of part of the stress to such a network. Indeed, experimental observations usually show that there is a critical concentration above which the stiffness increases abruptly.[16] In our previous work we observed some evidence of the transition to such mechanism in a nanotubes-filled rubber.[17] Another proposed mechanism is related to the presence of glassy layers around the nanoparticles,[18] which can significantly increase the stiffness of the system; this mechanism is applicable only if the temperature is close to the glass transition temperature of the matrix. Since the role of the above-mentioned mechanisms is still unclear, and other mechanisms are possible, the problem of the origins of reinforcement remains important for creation of new types of composites.

The properties of particle-reinforced polymer composites have been studied by computer simulations in a number of publications. Raos and Casalegno used dissipative particle dynamics (DPD) to study the nonequilibrium behavior—stress relaxation and oscillatory shear—of filled polymer networks containing solid spherical particles.[19,20] Sharaf and Mark studied the effect of different concentrations of nanoparticles on chain conformations in amorphous polyethylene melts using the Monte Carlo method.[21] Masnada et al. proposed a slip-link coarse-grained model to simulate entanglement-induced reinforcement in non-cross-linked composites.[22] Karatrantos et al. studied the effect of inclusion of carbon nanotubes into a melt of polymer chains on the entanglement length.[23] A comprehensive review about theory and simulation of polymer-based composites could be found in ref 24.

It should be noted, however, that for the moment there have been only few attempts to study the structural changes that occur in nanocomposites during deformation—such a study is relatively hard to conduct experimentally. However, it can give an insight into the true origins of reinforcement; computer simulation is a perfect tool to do that.

In our previous study[17] we proposed a model of a filled rubber and studied stress–strain responses of nanocomposites filled with nanotubes depending on their aspect ratio. In this work we tried to develop that approach further and study not only macroscopical characteristics (stress–strain response) but also microscopical changes which can influence on them. We studied elastomer matrixes filled with spherical particles, while deliberately avoiding an attempt to study a specific system. It should be noted that in order to understand the influence of nanoparticles on the structure of the matrix during deformation, one must know how the structure of a corresponding unfilled matrix behaves; therefore, we extensively studied such behavior before turning to nanocomposites.

2. METHODOLOGY

2.1. Simulation Method. DPD is a version of the coarse-grained molecular dynamics adapted to polymers and mapped onto the classical lattice Flory–Huggins theory.[25−28]

An ensemble of particles (beads) obeying Newton's equations of motion is considered:

$$\frac{d\mathbf{r}_i}{dt} = \mathbf{v}_i; \qquad m_i\frac{d\mathbf{v}_i}{dt} = \mathbf{f}_i$$
$$\mathbf{f}_i = \sum_{i\neq j}(\mathbf{F}_{ij}^{b} + \mathbf{F}_{ij}^{c} + \mathbf{F}_{ij}^{d} + \mathbf{F}_{ij}^{r}) \tag{2.1}$$

where $\mathbf{r}_i$, m_i, and $\mathbf{v}_i$ are the coordinate, mass, and velocity of an ith bead, respectively, and $\mathbf{f}_i$ is the force acting on it. The summation is performed over all other beads within the cutoff radius r_c. Below we assume that all quantities entering eq 2.1 are dimensionless and for simplicity set r_c and m_i for any i to unity. The first two terms in the sum are conservative forces.

Polymers are represented in terms of the bead-and-spring model. $\mathbf{F}_{ij}^{b}$ is a simple spring force describing the chain connectivity of beads:

$$\mathbf{F}_{ij}^{b} = -K(r_{ij} - l)\frac{\mathbf{r}_{ij}}{r_{ij}} \tag{2.2}$$

where K is a bond stiffness and l is the equilibrium bond length. If beads i and j are not connected, then $\mathbf{F}_{ij}^{b} = 0$.

$\mathbf{F}_{ij}^{c}$ is a soft core repulsion between ith and jth beads:

$$\mathbf{F}_{ij}^{c} = \begin{cases} a_{ij}(1 - r_{ij})\mathbf{r}_{ij}/r_{ij}, & r_{ij} \leq 1 \\ 0, & r_{ij} > 1 \end{cases} \tag{2.3}$$

where a_{ij} is a maximum repulsion between beads i and j attained at $r_{ij} = 0$. Since $\mathbf{F}_{ij}^{c}$ has no singularity at zero distance, a much larger time step than in the standard molecular dynamics could be used.

Other constituents of $\mathbf{f}_i$ are a random force $\mathbf{F}_{ij}^{r}$ and a dissipative force $\mathbf{F}_{ij}^{d}$ acting as a heat source and medium friction, respectively. They are taken as prescribed by the Groot–Warren thermostat in ref 28.

The use of soft volume and bond potentials leads to the fact that the bonds are formally "phantom", that is, capable of self-intersecting in three dimensions. The phantom nature of chains does not affect the equilibrium properties (for example, the chain gyration radius or the phase behavior of the system); moreover, it greatly speeds up the arrival of the system to equilibrium. However, if weakly cross-linked polymer networks are studied an explicit presence of entanglements is required. Nikunen et al.[29] described a method for rendering chains nonphantom in DPD without introduction of any additional conditions. It is based on geometrical considerations: if any two beads in the system cannot approach each other at a distance less than r_{min}, every unit in the system effectively has an excluded radius of $r_{min}/2$. If it is also assumed that each bond has a maximum length l_{max}, the condition of self-avoiding chains is

$$\sqrt{2}\, r_{min} > l_{max}$$

In our study we use $a_{ij} = 150$, $l = 0.5$, $k = 150$, and $\Delta t = 0.03$. In order to test if these parameters are sufficient for a chain to be

dx.doi.org/10.1021/ma500947g | Macromolecules 2014, 47, 5400−5408

nonphantom, we calculated the probability of chain self-intersection using the method described by Goujon et al.[30] This probability was found to be extremely small; i.e., the chains or subchains (their sections between cross-links) are not phantom.

2.2. System Generation and Stress−Strain Curves Calculation. All simulated systems were of the size 64^3 dimensionless (DPD) units with the bead number density of $\rho = 3$, therefore containing ∼800 000 beads.

In our work we used a coarse-grained model of a weakly cross-linked network (i.e., elastomer) which was used in our previous works.[17,31] To prepare the initial network configuration, we created a melt containing homogeneously distributed primary monodisperse polymer chains of the length N and pointlike cross-linkers with a functionality of 2, which can attach to any bead along a polymer chain, thus mimicking sulfur rings during rubber vulcanization. In this work for all systems N was equal to 1000; the cross-link density in the systems was varied through variation in the cross-linker concentration (number of cross-linker beads per chain). Assuming that each bead represents a statistical segment, $N = 1000$ for the case of polyisoprene results in the chains molecular weight of ∼100 kDa, which is reasonable from the experimental point of view.

After a short relaxation of 1×10^6 DPD steps, during which the parameters a and k were set 5 times lower in order to allow chains to self-intersect and reach the equilibrium state faster, the cross-linking process started. We assumed that every 200th DPD step the cross-linking beads could form irreversible bonds with randomly selected non-cross-linked neighboring polymer beads with a probability of 3×10^{-3}. Under these conditions, the equilibrium concentration fields remained approximately constant, and the chains had an equilibrium conformation during the cross-linking reaction. This process was repeated until 100% conversion was reached (at which all the cross-linker beads are bonded to two monomer units each); it took up to 4×10^5 DPD steps.

In order to test the effect of the network structure on its properties, we additionally created networks of two additional types: diamond-like and end-linked. In order to create a diamond-like structure, we simply placed all the beads on a diamond-like lattice and connected the closest beads to each other. Since such a lattice has an equal distance between junction points (which have functionality of 4), a network with no defects and the subchain length M was created. This type of networks is interesting because it is usually considered in theoretical studies.[1] It should be noted that the initial relaxation in the "phantom" regime allows such networks to be equilibrated in terms of entanglements. In what follows we call such networks "ideal". In order to create an end-linked network, we generated a melt of chains of the length M, in which 25% of the chain ends have functionality of 3. These chain ends could form bonds with the rest 75% of chain ends during the cross-linking process, therefore forming a network with the junction functionality of 4. One should note that despite having the same block-length distribution (delta-function), end-linked and diamond-like networks have some pronounced structural differences; namely, end-linked networks can contain defects (dangling ends, nonsaturated functionalities, and loops) and nonhomogeneous distribution of the junction points. See the Appendix for the results and discussion concerning this topic.

In order to study the properties of nanocomposites, spherical nanoparticles embedded into the matrix were used. Each particle had the diameter of 5 DPD units and contained 341 beads. In order to prepare a nanoparticle a spherical domain was cut out of a simple cubic lattice composed of beads; the lattice parameter of that lattice was equal to the mean bond length for our model. Each bead in such a structure was connected to the closest ones; therefore, the beads in the particles' cores had six bonds. Such structure is very rigid, and the nanoparticles did not change their shape during the simulations; it should be also noted that since the particles are not hollow and the potential used in our simulations forbids self-intersections, the polymer chains cannot penetrate into the particles. 15% of the beads on the filler particles surface were functionalized; these functionalized beads acted like cross-linker beads with functionality of 1 during the cross-linking process (i.e., they could form one bond with a non-cross-linked polymer bead). It should be noted that bonds between the particles surface and the matrix can be considered as an extreme case of strong adsorption. In order to avoid the effects related to the aggregation of the nanoparticles, they were initially placed on simple cubic lattice sites; the positions of their beads were not updated during the first relaxation phase and the cross-linking phase. During the stress−strain calculation phase the positions of those beads were integrated normally; however, in the studied systems the displacements of the nanoparticles were not big enough for them to aggregate. Figure 1 shows the initial arrangement of nanoparticles (top picture) and their positions after stretching (bottom picture) for a system containing 27 (3^3) nanoparticles.

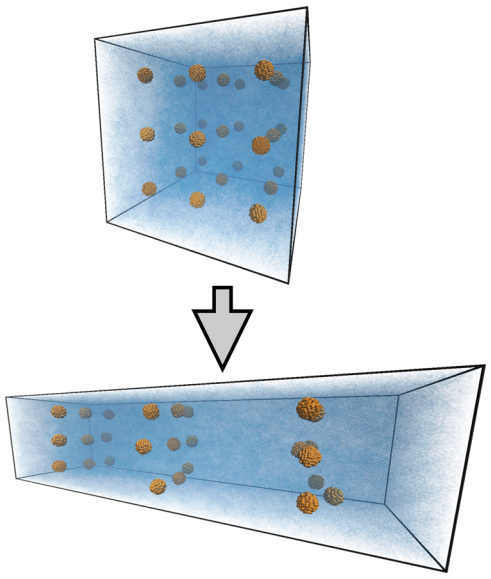

Figure 1. Snapshots of a system filled with 27 nanoparticles. Top: initial state; bottom: after stretching to $\lambda = 2.55$. The particles are depicted in orange, while the matrix is transparent and is shown in blue.

The strain−stress response was simulated under an uniaxial deformation of the simulation box along the x-axis preserving the box volume, i.e., in the incompressibility assumption. The system was deformed by changing the box size L_x in the x-direction to λL_{x0}, where λ stands for the extension ratio and L_{x0} is the initial box size before deformation. If a system is incompressible, for an uniaxial stretching along the x-axis one has $\lambda_x\lambda_y\lambda_z = 1$ and $\lambda = \lambda_x = \lambda_y^{-1/2} = \lambda_z^{-1/2}$; therefore, the system becomes compressed along the y- and z-axes. The transition to

dx.doi.org/10.1021/ma500947g | Macromolecules 2014, 47, 5400−5408

Table 1. Characteristics of the Systems under Study

system name	1	2	3	4	5	6	7	8
amount of cross-linker, beads per chain	8	16	32	64	128	16	16	16
amount of filler, beads per chain						12	58	178
mean active subchains length	64.5	33.2	16.6	8.2	4.1	32.5	29.9	24.8
mean length of subchains attached to the filler						29.3	28.5	25.2

a successive state (value of λ) consisted of two phases: (1) gradual deformation of the system, during which the positions of the beads were changed affinely, until the desired λ was reached; (2) long relaxation (12×10^6 DPD steps) at the desired strain λ. The components of the stress tensor $\mathbf{p}$ were calculated and averaged over the run of 3×10^6 time steps using the virial theorem:

$$p_{\alpha\beta} = \frac{1}{V}\sum_i v_{i\alpha}v_{i\beta} + \frac{1}{V}\sum_i\sum_{j>i}(F^c_{i\alpha} + F^b_{i\alpha})r_{ij\beta} \tag{2.4}$$

where V is the system volume, v_i is the velocity of ith bead, F^c_i and F^b_i are the soft repulsion and the bond force, respectively (see eq 2.1), and r_{ij} is the distance between ith and jth beads. The true stress t was calculated using the equation

$$t = \langle p_{xx}\rangle - \left\langle \frac{p_{yy} + p_{zz}}{2} \right\rangle \tag{2.5}$$

After the stress tensor averaging, the system was deformed to the next extension ratio λ. The process was repeated until the maximum λ of 2.81 was reached. See Figure 1 for the snapshots of a filled system in the initial state and the deformed state at λ = 2.55.

One should note that the used model does not take into account stress-induced crystallization (i.e., the chains cannot crystallize); therefore, it corresponds to a noncrystallizing rubber (like styrene−butadiene rubber). Moreover, due to a coarse-grained nature of the model, the only possible nonentropic (i.e., energetic) contribution to elasticity could be one related to stretching of the bond between beads; this contribution can be easily detected by studying the bond-length distribution. For more discussion concerning this topic see section 3.2.

2.3. Studied Systems and Their Structural Properties. Five unfilled systems with different cross-linker concentrations have been studied: 8, 16, 32, 64, and 128 cross-linker beads per chain. Characteristics of these systems are summarized in Table 1. For simplicity, in what follows we call these systems "systems 1−5" (see Table 1). The concentrations are given in "beads per chain" units; the total amount of beads corresponding to a certain fraction was divided by the total amount of polymer chain beads in the system.

The subchain statistics has an exponential form being in a perfect agreement with the previously reported data;[6,10] the presence of intramolecular cross-linking resulted in deviations in the limit of short subchains. The mean subchain length was calculated only for the elastically active subchains, i.e., excluding simple loops (simple loop is a subchain formed when two consecutive linking points on a chain are created by one cross-linker bead). It should also be noted that the minimal used cross-linker concentration of eight beads per chain is significantly higher than the percolation threshold obtained in ref 7; therefore, the fraction of dangling ends in the systems is relatively low—for system 1 only 14% of all polymer beads belong to the dangling ends, and this number becomes roughly 2 times lower when the cross-linker concentration is doubled.

To study the effect of network topology on the properties of unfilled network two additional systems were generated: with an ideal diamond-like structure and end-linked, with the subchain length M corresponding to system 2 (i.e., 33); see section 2.2 for more details concerning generation of these networks. They will hereinafter be referred as system 2d and system 2e, respectively.

Three filled systems with different filler volume fraction have been studied: with volume concentrations 1.18%, 5.43%, and 14.88%, which corresponds to 27, 125, and 343 particles, respectively (we call these systems "systems 6−8", see Table 1). In terms of the cross-linker beads concentration these systems correspond to system 2 (i.e., 16 beads per chain). As seen from Table 1, addition of the filler decreases the mean subchain length. It can be explained by the increased number of effective cross-links (as the filler particles surface is functionalized). The length statistics for subchains which are connected and not connected to the particles surfaces were found to be the same, as it was expected.

3. RESULTS AND DISCUSSION

3.1. Unfilled Networks: Stress−Strain Curves. Obtained stress−strain curves for the unfilled systems are presented in Figure 2. The choice of the abscissa axis in Figure 2a is related to the simple network elasticity theory, according to which true stress t is proportional to $(\lambda^2 - 1/\lambda)$.

To test if the stress−strain curves are equilibrium, we calculated reverse stress−strain curves starting from the most stretched state of λ = 2.81. Only system 1 exhibited a small hysteresis: the area under the stress−strain curve for compression is 7% smaller than for stretching. Presumably it can be explained by the presence of long dangling ends and more complex nonelastic structures due to a relatively small number of cross-linker beads per polymer chain, which greatly increases the relaxation time for the system; more detailed investigation of the observed hysteresis is out of the scope of this study. For systems 2−5 the difference between stretching and compression curves were smaller than averaging error.

To test the reproducibility of the results, five additional systems with the cross-linker concentration corresponding to system 2 were created starting from different initial random species distributions. The difference between obtained stress−strain curves and the stress−strain curve for system 2 was smaller than the averaging error (which is in turn smaller than the marker size in Figure 2a), indicating the systems under study are big enough to provide very good statistics.

As it was expected, increasing cross-linker concentration makes the system stiffer (see Figure 2a). Moreover, at high cross-linker concentrations stress−strain dependence becomes considerably nonlinear at large deformations. Mooney−Rivlin plots of the obtained curves are presented in Figure 2b; the curves for systems 4 and 5 are not shown. The curves in Figure 2b demonstrate two distinct regimes:

dx.doi.org/10.1021/ma500947g | Macromolecules 2014, 47, 5400−5408

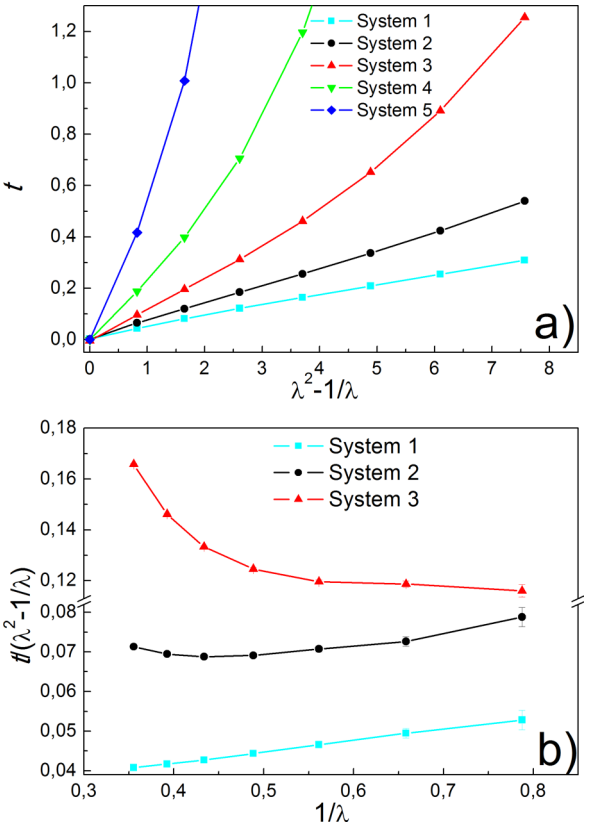

Figure 2. Stress–strain curves for randomly cross-linked unfilled networks with different amount of cross-linkers per chain: (a) standard plot and (b) Mooney–Rivlin plot. Averaging error in (a) is smaller than the marker size.

(a) Linear growth for systems 1 and 2 at small deformations ($\lambda < 2$). This behavior is consistent with the Mooney–Rivlin semiempirical law[32] $t = 2(\lambda^2 - \lambda^{-1})(C_1 + C_2/\lambda)$; the slope is equal to $2C_2$. In the Mooney–Rivlin semiempirical law C_1 is usually considered to be related to the density of subchains (and, therefore, to the cross-link density), while C_2 is generally believed to represent the contribution of entanglements.[33] The presence of this regime indicates that the subchains in a system are long enough to be entangled. It should be noted that for systems 1 and 2 the slope in Figure 1b is equal within the error range, which is consistent with experimental observations.[34]

(b) Nonlinear decay observed for systems 3–5 in the whole range of studied deformations (systems 4 and 5 are not presented in Figure 2b since the curves for them are similar to that for system 3, but lie significantly higher) and at $\lambda > 2$ for system 2. This behavior in noncrystallizing rubbers is usually attributed to the finite extensibility of the network chains, i.e., deviations from the Gaussian statistics of the subchains.[35] The absence of linear growth for systems 3–5 most probably indicates that there is a significant influence of short subchains on the properties of the systems.

3.2. Unfilled Networks: Segmental Orientation.

Coarse-grained particle models allow one to study orientation of segments explicitly, since a chain segment can be defined as a chain bond. According to the simple network elasticity theory, the relationship between the segmental (bond) orientation and the strain should be linear:[36]

$$\langle P_2(\cos(\alpha))\rangle = K_0(\lambda^2 - 1/\lambda) \quad (3.1)$$

where $\langle P_2(\cos(\alpha))\rangle = ((3\langle\cos^2\alpha\rangle - 1)/2)$, α is the angle between a chain segment and the principal axis of stretching, brackets denote statistical averaging, K_0 is equal to $(1/(5N))$ for the affine network model and to $(1/(5N))((1-2)/\phi)$ for the phantom network model, ϕ is the junction points functionality, and N is the subchain length. The obtained dependences of $\langle P_2\rangle$ on strain are depicted in Figure 3a.

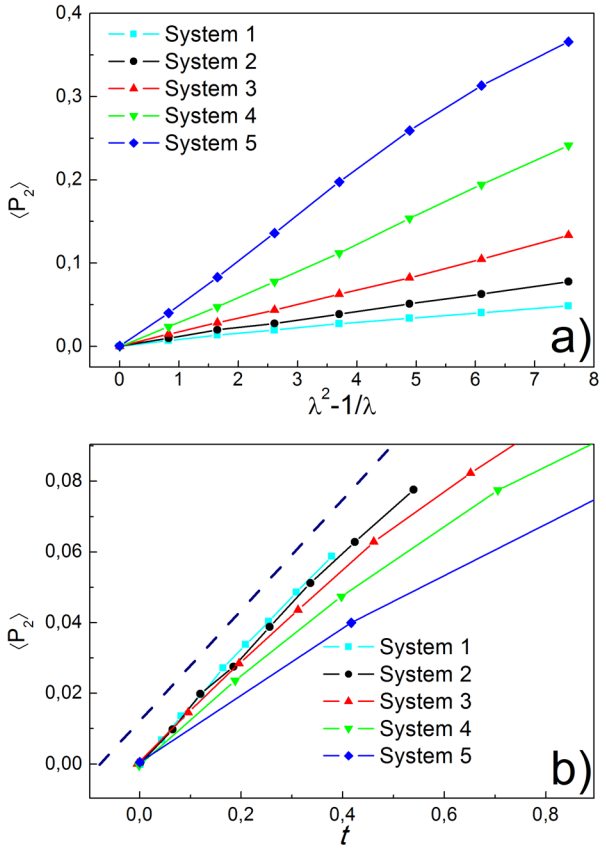

Figure 3. Dependences of the segmental orientation on strain (a) and true stress (b).

$\langle P_2\rangle$ varies linearly with $((\lambda^2 - 1)/\lambda)$ for all systems but system 5. In order to explain this deviation from linearity, we checked if system 5 is still in the entropic regime of elasticity, and we found out that for deformations $\lambda > 2$ for this system the bonds between beads start to stretch (compared to the unstratched sample), indicating a transition to the nonentropic regime; for system 4 such deviations were found at $\lambda = 2.81$ (i.e., for $((\lambda^2 - 1)/\lambda) = 7.57$). For systems 1–3 the bond length distribution remained the same for all deformations, indicating pure entropic regime of elasticity. The linearity of the curves for systems 1–4 in Figure 3a is consistent with the experimental data[5] and however seems surprising: it holds even for systems 3–4, properties of which, according to the mechanical tests in section 3.1, are controlled by chains with non-Gaussian statistics. It becomes even more surprising considering the fact that eq 3.1 is valid only for relatively long chains (for short chains the dependence of $\langle P_2\rangle$ on $((\lambda^2 - 1)/\lambda)$ becomes noticeably nonlinear due to the higher-order corrections),[36] whereas all studied systems contain big amount of short subchains (since the subchain length distribution is exponential), and for systems 3–4 even the mean subchain length (see Table 1) is too small for eq 3.1 to be valid. A

dx.doi.org/10.1021/ma500947g | Macromolecules 2014, 47, 5400–5408

possible explanation for that is some rearrangements in the network structure; for further discussion see section 3.3.

According to the general theory of viscoelasticity of polymer liquids, the microscopic expression for the stress tensor can be written as follows:[37]

$$p_{ij} = \frac{3k_bT}{Vb^2} \sum_{\text{all segments}} \langle r_{ni} r_{nj} \rangle \approx 3k_bT\rho\langle \cos(\alpha_i)\, \cos(\alpha_j)\rangle,$$

$$i,\ j = x,\ y,\ z \qquad (3.2)$$

where b is the statistical segment length, V is the system volume, r_{ni} and r_{nj} are the ith and jth components of nth segment (bond), respectively, ρ is the segment number density, and α_i and α_j are the angles between a segment and the axes i and j, respectively (brackets denote averaging). Combining eqs 3.2 and 2.5, in the case of uniaxial stretching one gets

$$t = 3k_bT\rho\langle P_2(\cos(\alpha))\rangle \qquad (3.3)$$

This equation is quite general; it should hold for any system (including entangled ones) with Gaussian chain statistics.[37] In Figure 3b the dependences of $\langle P_2 \rangle$ on t are shown. It is apparent that the curves are linear only for system 1 and system 2 at small stresses, which is consistent with the conclusions made in section 3.1—for systems 3−5 and system 2 at $\lambda > 2$ the properties are controlled by chains with non-Gaussian statistics. It should be also noted that for system 1 and system 2 at $\lambda < 2$ eq 3.1 should not be valid, since $\langle P_2 \rangle$ is proportional to t according to eq 3.3, and the dependence of t on $((\lambda^2 - 1)/\lambda)$ is nonlinear (see Figure 2b). However, due to rather small Mooney−Rivlin coefficient C_2, these curves in Figure 3a might look linear.

3.3. Unfilled Networks: Redistribution of Deformations and Orientations of the Subchains. The concept of redistribution of deformations between subchains of different length was proposed by Andrady et al.[34] as a result of study of the mechanical properties of networks with bimodal subchain length distribution. Figure 4a shows the averaged ratio of squared end-to-end distance in the deformed state to the same quantity in the undeformed state $\langle R_e^2/R_{e0}^2 \rangle$ for different subchain lengths. It should be noted that $\langle R_e^2 \rangle$ is the only parameter the stress in the simple theory of elasticity is dependent on,[1] but for entangled systems the situation is somewhat more complex. However, the ratio $\langle R_e^2/R_{e0}^2 \rangle$ seems to be a good choice to study structural rearrangements in the matrix.

Figure 4a shows that the subchains in the samples are stretched differently: the longer the subchain, the more it is deformed (probably, there is saturation in the limit of very long subchains). In the weakly cross-linked systems (systems 1 and 2) short subchains are not stretched at all. Such behavior is predicted by the tube models[2,10] and can be interpreted as redistribution of deformations between subchains of different length: longer subchains are stretched more to release some stress on shorter ones. Increase in the cross-linker concentration leads to involving shorter chains to the deformation process and increasing the overall subchains stretching. If many short subchains are involved to the deformation process, the system demonstrates a transition to non-Gaussian regime of the stress−strain response (regime b in section 3.1). The same process is observed for the subchains orientation $\langle P_2^R(\cos(\theta))\rangle$, which is calculated using the angle between the axis of deformation and the end-to-end vector of a subchain θ (Figure 4b). These data indicate a highly nonaffine deformation of the matrix junction points and overall complexity of the structural rearrangements during network stretching.

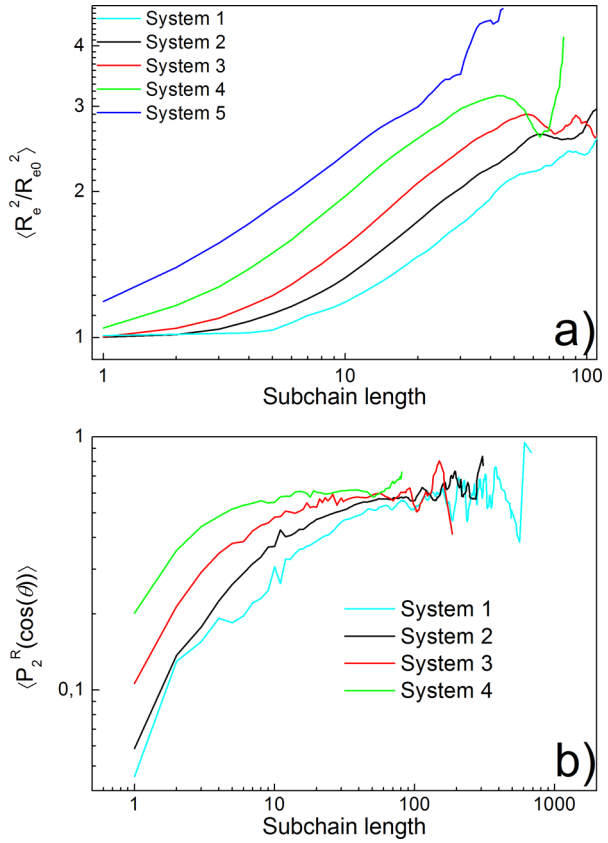

Figure 4. Dependence of (a) the relative increase of the squared mean end-to-end vector R_e compared to the same in the nonstretched sample R_{e0} and (b) the mean end-to-end vector orientation (system 5 is not shown since it is in the nonentropic regime of deformation) on subchain length at $\lambda = 2.81$. The curves were smoothed for better appearance. The scatter at large subchain lengths is related to the small amount of those subchains.

3.4. Filled Networks: Stress−Strain Curves. Figure 5 shows stress−strain curves for the systems containing spherical nanoparticles (systems 6−8) compared to the unfilled ones (systems 2−4). Similarly to system 2, for the filled systems no hysteresis was observed.

The reinforcement is apparent from Figure 5—increase in the filler concentration makes the system stiffer. It also should be noted that system 8 is stiffer than system 3, whereas the mean chain length for system 3 is much smaller. Moreover, Figure 5b shows that inclusion of NPs shifts the upturn in the Mooney−Rivlin plot toward small deformations, which cannot be explained by the change in the mean subchain length (see Table 1). As it was mentioned in section 3.1, the upturn is usually attributed to the finite chain extensibility, so the reason for the shift must be in the structural changes.

3.5. Filled Networks: Segmental Orientation. Figure 6a shows the obtained dependences of $\langle P_2(\cos(\alpha))\rangle$ on strain for the filled systems compared to the unfilled ones. Again, the dependences are linear; small deviations from the entropic behavior (based on stretching of individual bonds, see section 3.2) were observed only for system 8 at $\lambda = 2.81$. The linearity of the dependences for the filled systems is consistent with the

dx.doi.org/10.1021/ma500947g | Macromolecules 2014, 47, 5400−5408

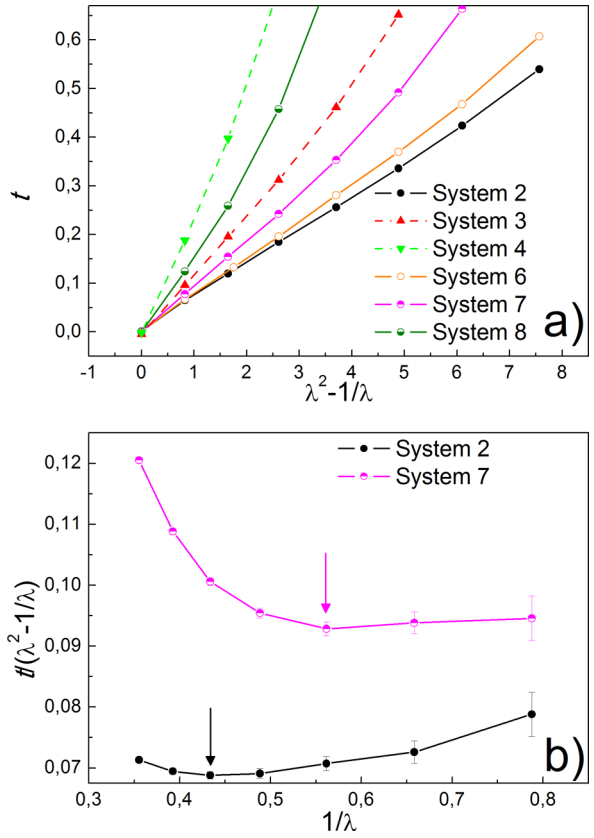

Figure 5. Stress–strain curves for randomly cross-linked networks with different amount of filler compared to unfilled systems: (a) standard plot and (b) Mooney–Rivlin plot. The arrows show the beginning of the upturn.

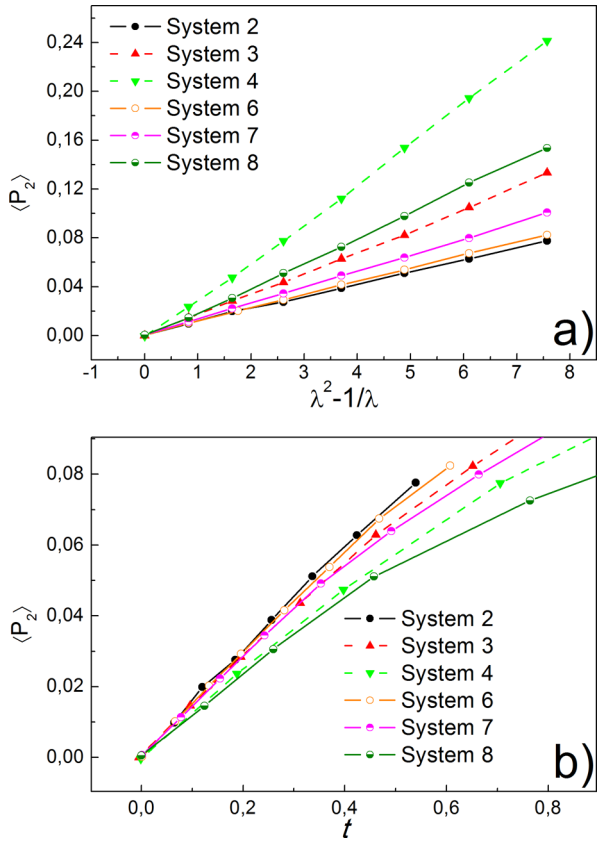

Figure 6. Dependences of the segmental orientation on strain (a) and true stress (b).

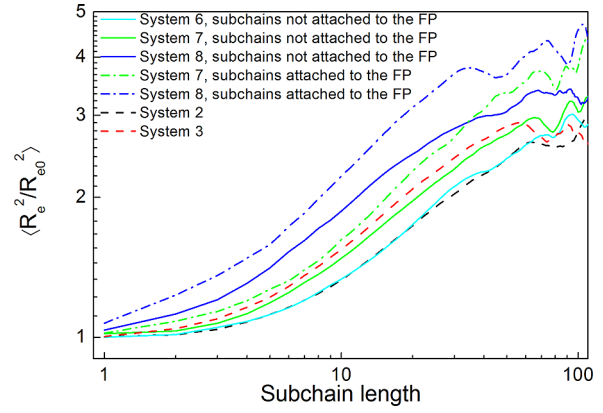

Figure 7. Dependence of the relative increase of the squared mean end-to-end vector R_e compared to the same in the nonstretched sample R_{e0} on subchain length at $\lambda = 2.81$. FP stands for "filler particles". The curves were smoothed for better appearance. The scatter at large subchain lengths is related to the small amount of those subchains.

experimental data;[16] however, the discussion given in section 3.2 is valid for these systems as well.

Figure 6b which shows the dependence of $\langle P_2(\cos(\alpha))\rangle$ on t reveals an important feature: system 8, being softer than system 4 (see Figure 5a), shows stronger deviation from linearity (eq 3.2) than system 4. Since we do not observe changes in the bond-length distribution up to $\lambda = 2.81$, this deviation cannot be explained by a nonentropic contribution. Therefore, the structural changes must be studied to reveal the underlying reason for the deviation.

3.6. Filled Networks: Redistribution of Deformations of the Subchains. Since in our model the surface of the filler particles is functionalized (see section 2.2), there exist two types of subchains: connected (at least with one end) and not connected to the surface of a particle. Figure 7 shows the dependence of $\langle R_e^2/R_{e0}^2\rangle$on the subchain length for these different types of subchains.

It is seen from Figure 7 that the subchains in the filled with significant amount of NPs systems (namely systems 7 and 8) are stretched much more than in unfilled system with the same cross-linker concentration. This effect has been extensively studied in some recent publications[13,38] and is commonly referred to as strain amplification, since the matrix containing undeformable filler particles must be deformed more to reach the same macroscopic extension ratio as the corresponding unfilled matrix; it explains the observed shift of the upturn in Figure 5b. However, Figure 7 shows that the chains attached to the filler particles are even more deformed; the reason is presumably the low mobility of the attached subchain ends, which can deform only affinely; subchain deformations in the affine network model are higher than in the models where the chain ends can fluctuate,[1] resulting in a more rigid behavior. Therefore, the feature observed in section 3.5 can be attributed to the presence of subchains attached to the nanoparticles: since those subchains are more deformed, deviations from Gaussian behavior are more pronounced for them—their segments are oriented less than it would be expected from the stress they bear due to their non-Gaussian statistics; this means that the overall (average) segmental orientation is lower than it

dx.doi.org/10.1021/ma500947g | Macromolecules 2014, 47, 5400–5408

would be expected from the observed macroscopic stress (Figure 6b). It should be noted again that apart from system 8 at $\lambda = 2.81$ (see section 3.5) we did not observe any deviations from the entropic behavior either for attached or not attached subchains. Fraction of the attached chains increases along with the filler concentration, providing nonlinear reinforcement. One should note that the properties of chains not connected to the nanoparticles may differ depending on how close to the connected ones in terms of connectivity such chains are; however, such differences should be not as pronounced as those between connected and not connected in general. Thus, the microscopic behavior of the matrix in filled elastomers is even more complicated than in unfilled ones (discussed in sections 3.2 and 3.3) due to the presence of several sets of subchains with distinct behavior. If the filler concentration is high enough, the areas of the subchains affected by the filler surfaces may overlap, resulting in abrupt increase of the modulus (which is usually attributed to "filler percolation"). It should be also noted that probability of scission is higher for a stretched chain as well. Therefore, in this work we show that the only reason for reinforcement for our systems is changes in the properties of the matrix alone, which is consistent with the mechanism proposed in ref 14.

4. CONCLUSIONS

In this work we used dissipative particle dynamics simulations to gain insight into the connection between mechanical properties and the structure of cross-linked elastomers filled with spherical particles. In order to understand the influence of the nanoparticles, a rigorous study of the structural properties of unfilled matrixes was carried out, and then their behavior was compared to the behavior of the corresponding filled systems. The random networks were obtained via chain cross-linking reaction (model of sulfur vulcanization) in the presence of spherical particles having reactive surface sites capable of bonding irreversible with polymer matrix. The mechanical properties of the composites were investigated under uniaxial stretching; all the obtained stress−strain curves were at equilibrium or close to equilibrium, which is confirmed by the absence of hysteresis. One of the main achievements of this study was a possibility to create rather big systems with a good subchain statistics and subchain lengths reasonably big.

Five unfilled systems with different cross-linker concentration were studied. As it was expected, increasing cross-linker concentration makes the system stiffer; at high cross-linker concentrations stress−strain dependence becomes considerably nonlinear at large deformations. Two systems with the lowest cross-linking degree show a linear rise in a Mooney−Rivlin plot, which is consistent with the available experimental data and is usually attributed to the presence of entanglements. The dependences of segmental orientation $\langle P_2(\cos(\alpha))\rangle$ on $((\lambda^2 - 1)/\lambda)$ were found to be linear for all systems which were in the entropic regime; however, such linearity is surprising because it holds even for the systems the properties of which were controlled by chains with non-Gaussian statistics. Moreover, since the randomly cross-linked networks contained a lot of short chains for which the dependence of $\langle P_2(\cos(\alpha))\rangle$ on $((\lambda^2 - 1)/\lambda)$ should be nonlinear, we assumed that there was a redistribution of deformation and orientation between subchains of different length. The dependences $\langle P_2\rangle$ on t collapsed on a same linear master curve for the systems with Gaussian chain statistics and showed negative deviations from the linearity when the statistics became non-Gaussian, which is consistent with the available experimental data. In order to study the structural rearrangements in the matrixes, we calculated the averaged ratio of squared end-to-end distance in the deformed state to the same quantity in the undeformed state for different subchain lengths; we found that the longer the subchain, the more it is deformed, i.e., longer subchains are stretched more to release some stress on shorter ones. This fact is predicted by the tube models of rubber elasticity and can be interpreted as redistribution of deformations between subchains of different length. Increase in the cross-linker concentration leads to involving shorter chains to the deformation process and increasing the overall subchains stretching. The same process is observed for the subchains orientation, which was calculated using the angle between the axis of deformation and the end-to-end vector of a subchain.

Having studied the structural properties of the unfilled matrixes, we turned to the properties of composites. Non-aggregated spherical particles with functionalized surface (which can be considered as an extreme case of strong adsorption) were used as the filler; three different filler fractions were studied. It was found that one of the filled systems is stiffer than one of the unfilled even considering the fact that the mean subchain length is 1.5 times smaller for the unfilled network. It was also observed that inclusion of nanoparticles shifts the upturn in the Mooney−Rivlin plot toward small deformations, which cannot be explained by the change in the mean subchain length. The dependences of $\langle P_2(\cos(\alpha))\rangle$ on $((\lambda^2 - 1)/\lambda)$ for the filled systems were found to be linear; all the conclusions made for unfilled systems are valid for this case as well. The dependence of $\langle P_2(\cos(\alpha))\rangle$ on t revealed an important feature: one of the filled systems, being softer than one of the unfilled ones, shows stronger deviation from linearity than the unfilled one. The explanation of such behavior lies in the strong heterogeneity in the structural properties of the nanocomposites: there are several sets of subchains with distinct properties. Part of the subchains which are not connected to the filler particles are deformed slightly more than in the unfilled matrix; the subchains connected (absorbed) to the filler particles are deformed significantly more. Therefore, the observed feature of the segmental orientation can be attributed to the presence of several sets of subchains: subchains attached to the nanoparticles are more deformed than not attached; deviations from Gaussian behavior are more pronounced for them—their segments are oriented less than it would be expected from the stress they bear due to their non-Gaussian statistics, which means that the overall (average) segmental orientation is lower than it would be expected from the observed macroscopic stress. If the filler concentration is high enough, the areas of the subchains affected by the filler surfaces may overlap, resulting in abrupt increase of the modulus.

Summarizing, in this work we have shed some light on the molecular mechanisms of the filler reinforcement; this is critical for creating new types of nanocomposites with improved properties.

APPENDIX

Unfilled Networks: Matrixes with Different Structures but the Same Mean Subchain Length

Figure 8 shows comparison of mechanical properties of networks with different structures but the same mean subchain length ($\bar{N} = 33$).

dx.doi.org/10.1021/ma500947g | Macromolecules 2014, 47, 5400−5408

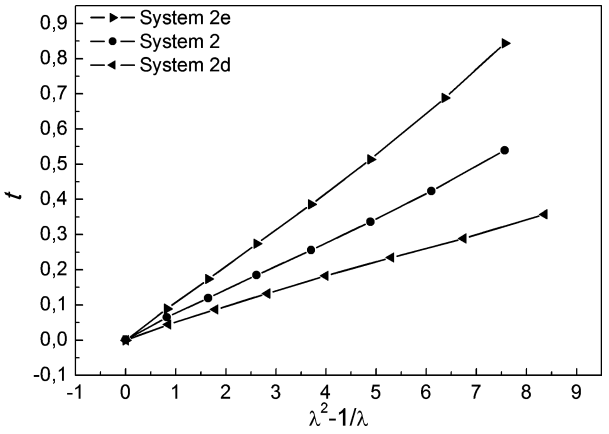

Figure 8. Comparison of mechanical properties of networks with different structure.

System 2e (end-linked network) is stiffer than system 2 (randomly cross-linked), in line with the results of Svaneborg et al.[10] They explained this fact by the increased tube diameter for the randomly cross-linked networks, i.e., decreased influence of the entanglements, which probably can be explained by different subchain length statistics—in the randomly cross-linked network there are many short unentangled subchains. System 2d (diamond-like network), on the other hand, is softer than system 2, presumably due to significantly reduced squared end-to-end distance (16.6 compared to 25.8) of the subchains with the mean length $\bar{N}$ = 33; so, in the initial state the subchains in system 2d are compressed, which results in softer behavior. This can be explained by the lack of defects in system 2d, which does not allow the subchains to relax completely. To test the effect of the number density, we generated two additional pairs of structures (randomly cross-linked and diamond-like) with densities ρ = 1 and 2; the subchains in the diamond-like networks were always compressed. The dependences of true strain on segmental orientation (eq 3.3) have confirmed this hypothesis: whereas the curves for systems 2 and 2e collapse well on a master curve, the curve for system 2d has significantly larger slope, indicating deviations from Gaussian statistics due to subchains compression (in contrast with the behavior of systems 3−5 for which the slope is smaller due to the chains extension).

AUTHOR INFORMATION

Corresponding Author

*E-mail gavrilov@polly.phys.msu.ru (A.A.G.).

Notes

The authors declare no competing financial interest.

ACKNOWLEDGMENTS

The financial support from RSCF (grant no.14-23-00161) is appreciated. We thank Moscow State University Supercomputer Center[39] for providing the computational resources.

REFERENCES

(1) Rubinstein, M.; Panyukov, S. *Macromolecules* **2002**, *35*, 6670−6686.
(2) Mergell, B.; Everaers, R. *Macromolecules* **2001**, *34*, 5675−5686.
(3) Erman, B. *Curr. Opin. Solid State Mater. Sci.* **2010**, *14*, 35−37.
(4) Davidson, J. D.; Goulbourne, N. C. *J. Mech. Phys. Solids* **2013**, *61*, 1784−1797.
(5) Vieyres, A.; Perez-Aparicio, R.; Albouy, P.-A.; Sanseau, O.; Saalwächter, K.; Long, D. R.; Sotta, P. *Macromolecules* **2013**, *46*, 889−899.
(6) Grest, G. S.; Kremer, K. *Macromolecules* **1990**, *23*, 4994−5000.
(7) Grest, G. S.; Kremer, K. *J. Phys. (Paris)* **1990**, *51*, 2829−2842.
(8) Everaers, R.; Kremer, K. *Macromolecules* **1995**, *28*, 7291−7294.
(9) Svaneborg, C.; Grest, G. S.; Everaers, R. *Phys. Rev. Lett.* **2004**, *93*, 257801.
(10) Svaneborg, C.; Grest, G. S.; Everaers, R. *Polymer* **2005**, *46*, 4283−4295.
(11) Svaneborg, C.; Grest, G. S.; Everaers, R.; Gurro, J. *Macromolecules* **2008**, *41*, 4920−4928.
(12) Bokobza, L. *Polymer* **2007**, *48*, 4907−4920.
(13) Bokobza, L. *Macromol. Mater. Eng.* **2004**, *289*, 607−621.
(14) Sternstein, S. S.; Zhu, A.-J. *Macromolecules* **2002**, *35*, 7262−7273.
(15) Riggleman, R. A.; Toepperwein, G.; Papakonstantopoulos, G. J.; Barrat, J.-L.; de Pablo, J. J. *J. Chem. Phys.* **2009**, *130*, 244903.
(16) Perez-Aparicio, R.; Vieyres, A.; Albouy, P.-A.; Sanseau, O.; Vanel, L.; Long, D. R.; Sotta, P. *Macromolecules* **2013**, *46*, 8964−8972.
(17) Gavrilov, A. A.; Chertovich, A. V.; Khalatur, P. G.; Khokhlov, A. R. *Soft Matter* **2013**, *9*, 4067−4072.
(18) Berriot, J.; Montes, H.; Lequeux, F.; Long, D. R.; Sotta, P. *Macromolecules* **2002**, *35*, 9756−9762.
(19) Raos, G.; Moreno, M.; Elli, S. *Macromolucules* **2006**, *39*, 6744−6751.
(20) Raos, G.; Casalegno, M. *J. Chem. Phys.* **2011**, *134*, 054902.
(21) Sharaf, M. A.; Mark, J. E. *Polymer* **2004**, *45*, 3943−3952.
(22) Masnada, E.; Merabia, S.; Couty, M.; Barrat, J.-L. *Soft Matter* **2013**, *9*, 10532−10544.
(23) Karatrantos, A.; Clarke, N.; Composto, R. J.; Winey, K. I. *Soft Matter* **2013**, *9*, 3877−3884.
(24) Allegra, G.; Raos, G.; Vacatello, M. *Prog. Polym. Sci.* **2013**, *33*, 683−731.
(25) Hoogerbrugge, P. J.; Koelman, J. M. V. A. *Europhys. Lett.* **1992**, *19*, 155−160.
(26) Schlijper, A. G.; Hoogerbrugge, P. J.; Manke, C. W. *J. Rheol.* **1995**, *39*, 567−579.
(27) Espanol, P.; Warren, P. B. *Europhys. Lett.* **1995**, *30*, 191−196.
(28) Groot, R. D.; Warren, P. B. *J. Chem. Phys.* **1997**, *107*, 4423−4435.
(29) Nikunen, P.; Vattulainen, I.; Karttunen, M. *Phys. Rev. E* **2007**, *75*, 036713.
(30) Goujon, F.; Malfreyt, P.; Tildesley, D. J. *J. Chem. Phys.* **2008**, *129*, 034902.
(31) Gavrilov, A. A.; Chertovich, A. V. *Polym. Sci., Ser. A* **2014**, *56*, 90−97.
(32) Mooney, M. A. *J. Appl. Phys.* **1940**, *11*, 582−592.
(33) Wagner, M. H. *J. Rheol.* **1994**, *38*, 655−679.
(34) Andrady, A. L.; Llorente, M. A.; Mark, J. E. *J. Chem. Phys.* **1980**, *72*, 2282−2290.
(35) Mark, J. E. *J. Phys. Chem. B* **2003**, *107*, 903−913.
(36) Erman, B.; Mark, J. E. *Structure and Properties of Rubberlike Networks*; Oxford University Press: New York, 1997.
(37) Doi, M., Edwards, S. F. *The Theory of Polymer Dynamics*; Oxford University Press: New York, 1988.
(38) Pérez-Aparicio, R.; Schiewek, M.; López Valentín, J.; Schneider, H.; Long, D. R.; Saphiannikova, M.; Sotta, P.; Saalwächter, K.; Ott, M. *Macromolecules* **2013**, *46*, 5549−5560.
(39) http://hpc.msu.ru.